Article

Implantation of Elongated Porous Silicon Neural Probe Array in Rat Cortex

Mohamad Hajj-Hassan[1]*, Rayan Fayad[1], Soumaya Berro[1], Vamsy P. Chodavarapu[2], Sam Musallam[3]

[1] Department of Biomedical Engineering, Lebanese International University, Mazraa, Beirut, P.O.Box 146404, Lebanon
[2] Department of Electrical and Computer Engineering, University of Dayton, 300 College Park, Dayton, Ohio, 45469, USA
[3] Department of Electrical and Computer Engineering, McGill University, 3480 University Street, Montreal, Quebec, H3A2A7, Canada
* Correspondence: mohamad.hajjhassan@liu.edu.lb; 10930639@students.liu.edu.lb; soumaya.berro@liu.edu.lb; vchodavarapu1@udayton.edu; sam.musallam@mcgill.ca; Tel.: 1-937-229-2780

Abstract: Neural microprobes represent an important component of neural prosthetic systems where implanted microprobes record the electro-potentials generated by specific thoughts in the brain and convey the signals to algorithms trained to interpret these thoughts. Here, we present novel elongated multi-site neural probe that can reach depths greater than 10mm. We hypothesize that reaching such depth allows the recording of cognitive signals required to drive cognitive prosthetics. The impedance of the recording sites on the probes was on the order of 500 kΩ at 1 kHz, which is consistent with probes used for neurophysiological recordings. The probes were made porous using Xenon Difluoride (XeF_2) dry etching to improve the biocompatibility and their adherence to the surrounding neural tissue. Numerical studies were performed to determine the reliability of the porous probes. We implanted the elongated probe in rats and show that the elongated probes are capable of simultaneously recording both spikes and local field potentials (LFPs) from various recording sites.

Keywords: cognitive neural prosthetics; brain machine interfaces; porous silicon; microprobes

PACS: J0101

1. Introduction

Brain Machine Interfaces (BMIs) have the potential to improve the lives of paralyzed patients by allowing them to use their neural activity to operate computers, robots, or even their own limbs [1, 2]. BMIs are designed to function in real time and benefit from real or simulated feedback. The development of BMIs as a direct communication pathway between the brain and external devices has generated novel methods and techniques to interface with and to study the brain [2]. A BMI platform is comprised of 1) a system to record neural signals, 2) algorithms to interpret the neural signals and 3) the device to be controlled. In this paper, we focus on recording platforms composed of multiple probes implanted in the brain. These platforms must be biocompatible, designed to minimize the short term and long term trauma inflicted during and after insertion. The probes must also be long enough to reach variable depths. Thus, probes must be made durable without increasing their width. Implantable probe arrays have traditionally been metal microprobes [3-5]. However, these have been recently supplanted by silicon probes [6-12]. Implanting probes into the brain elicits a tissue response

 doi:10.20944/preprints201801.0080.v1

that degrades the recorded signals. Regardless of substrate, probe design must curtail this response to ensure long-term recording.

Relative movement of the probes within the brain causes long-term tissue response due to the difference in mechanical properties between the probes and the neural tissue [13-15]. This process is exacerbated by arrays implanted deep in the brain due to their longer moment arm. Silicon probes can be made thin enough to increase compliance in the brain but without some rigidity, thin probes cannot penetrate neural tissue. Devices to assist implantation have been tested but may still cause neural damage during insertion and can only be used for surface arrays [16, 17].

We previously researched methods to develop implantable arrays made from silicon that can record signals from areas that are 6.5mm beneath the brain [18, 19]. Considerable progress in the design and fabrication of elongated silicon probes that can reach depths in the brain required for our applications were made. Silicon probes were reinforced probes with metallic structures making them more stable [10].

2. Tissue response

The neural injury incurred by probe implantation compromises the integrity of the recorded signals [13, 20, 21]. Immune cells isolate the foreign objects by forming as a sheath around the probe [21, 22]. This isolates the probes to decrease inflammation, and inhibits axon growth. This scaring stabilizes after several weeks [23]. However, recorded signals continue to degrade. The continued presence of the probes leads to persistent inflammation and process that continually damage tissue perpetuating neural loss [24].

Signal degradation can be mitigated by reducing the formation of the glial scar by reducing the immune response, or by the addition of proteins that encourage neural growth around the probe [24-27]. Neural probes impregnated with neural growth factors represent an alternative approach to promote the growth of neurons surrounding the probe [28]. Neurotrophic probes have had much success, particularly in humans, where they have been able to isolate single units for over 4 years [29-31].

Previously, our group has shown nanostructured porous silicon (PSi) surface for implants were showed to improve biocompatibility [32]. Here, we report the use of porous silicon scaffolds, fabricated using Xenon Difluoride (XeF2) dry etching technique, to improve the biocompatibility of the neural probe.

3. Design and Simulation of the Porous Probe

Using microfabrication processes, silicon-based neural probes have well-defined probes holding accurately distributed and spaced recording sites [18]. We manufactured elongated silicon neural probes that can reach 10.5 mm deep into the brain. Figure 1(a) illustrates a single protruding tapered silicon probe that is part of the proposed neural microprobe array consisting of 4 μm probes (as shown in Figure 1(b)) [10, 19]. Each neural probe holds three metallic recording sites to record brain electrical activity, interconnect traces, and back carrier area holding the bonding pads to connect the probes to external read-out electronics. The thickness of the probe array is 50 μm. The length of the probe is 10.5 mm and is divided into a tapered support base region, a measuring region, and a piercing region which are 250 μm, 10 mm, and 250 μm respectively. The tapered base, 350 μm wide, is meant to offer enough strength for each neural probe to withstand surgical implantation. The width of the measuring region gradually reduces along the length of the neural probe in order to minimize brain tissue damage. This region carries several 10 μm x 10 μm gold recording sites to measure neural electrical activities at different depths. To allow an easy entry into the brain, the tip of the neural probe, or piercing region, was shaped into a chisel tip. The distance between the two neighboring probes is 350 μm.

Preprints (www.preprints.org) | NOT PEER-REVIEWED | Posted: 9 January 2018 doi:10.20944/preprints201801.0080.v1

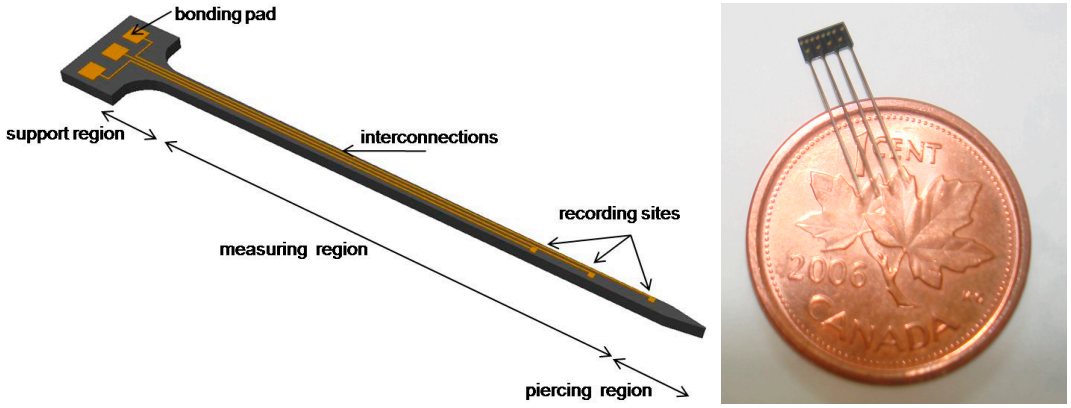

(a) (b)

Figure 1. (a) Design of a single probe probe carrying the recording sites, interconnects, and bonding pads. (b) Photomicrograph for the complete fabricated probe array which consisting of four silicon probes.

In order to investigate the mechanical strength of the probe, a Finite Element Method (FEM) model of the probe was generated and simulated with the MEMS module in COMSOL Multiphysics. The properties of the silicon used to manufacture the probes were entered into COMSOL. The model structure was meshed into tetrahedral elements with an element size of 4 μm, which was selected so that the simulation converges towards a unique solution. In Figure 2, a layer of porous silicon covers the surface of the probe. The regions of the connecting wires and metal sites are left nonporous. The purpose behind the simulation was to find the failure stresses of the probe due to the forces exerted during and after implantation. The effect of porosity on the mechanical strength of the probe was investigated, due to the fact that the pores represent micro defects that might cause failure. The forces were applied at the tip of the probe since it experiences the most stress during implantation. The imposed forces can be classified into three different cases: (1) under application of two axial forces which are imposed during the penetration phase of the implantation process, (2) under application of a single axial force which occurs directly after penetration and may cause the buckling of the probe, and (3) under application of a vertical force which occurs after the probe implementation and may result in the bending of the probe. In all the 3 cases, the maximum critical stress was yielded by applying increasing stress to the tip of the probe (while fixing its base) until a certain von Mises stress is reached, which is equivalent to the yield stress of a thin silicon cantilever that is approximately equal to 1 GPa [10]. The FEM model of a nonporous probe was used for comparison during all testing cases. For each simulation, a color map of the induced von Mises stress in MPa illustrating the accumulation of the induced stresses on the surface of the probes is plotted.

 doi:10.20944/preprints201801.0080.v1

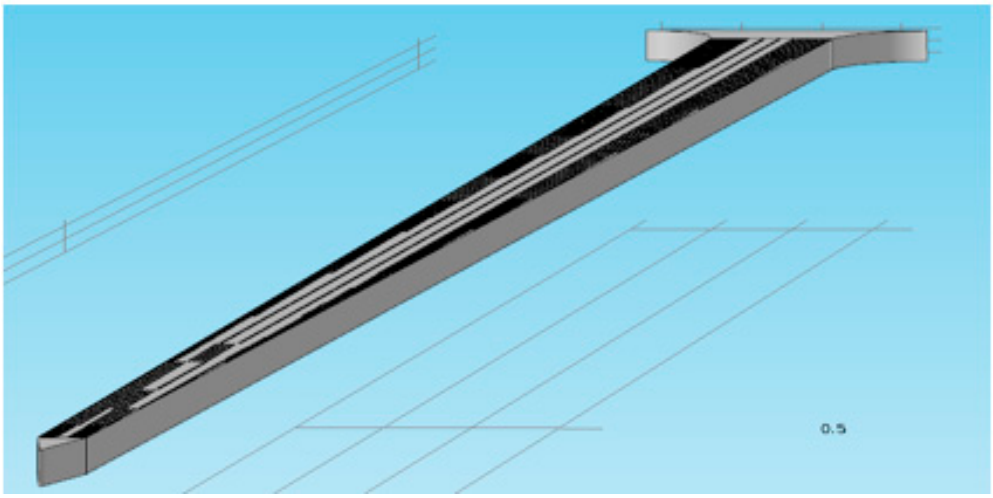

Figure 2. 3D model of the porous probe.

In case 1, for the non-porous probe a stress of 756 MPa induced the yield stress (1 GPa) at the middle and the tip of the probe as depicted in Figure 3. For the same case, for the porous probe, a stress of 753.7 MPa induced the 1 GPa yield stress in the probe as depicted in Figure 4. In case 2, a stress of 1055 MPa induced the yield stress (1 GPa) at the tip of the probe. As for the porous probe, a stress of 1045 MPa induced the same yield stress. In case 3, a stress of 36.5 MPa induced the yield stress (1 GPa) at the base of the probe as depicted in Figure 5. As for the porous probe, a stress of 23 MPa induced the same yield stress as depicted in Figure 6. First, a direct comparison of the forces that induced the maximum yield stress in the 3 different cases, one can notice the mechanical weakening of the porous silicon probe. The weakening was 0.3 %, 0.1%, 37% in cases 1, 2 and 3 respectively. Nonetheless, this weakening does not significantly risk the mechanical integrity of the neural probe, and this is due to the reason that the force that induced the maximum yield stress of the porous probe is still much higher than the minimum force that the probe must withstand during the penetration of the brain tissue especially for the most significant case 2 (~5MPa [10]). Table 1 summarizes all the simulations conducted for the three cases for porous and non-porous probes. Using the induced stress and the location of application (area of the tip of the probe is 50 μm by 10 μm) the maximum forces endured by the probe can be calculated.

Preprints (www.preprints.org) | NOT PEER-REVIEWED | Posted: 9 January 2018 doi:10.20944/preprints201801.0080.v1

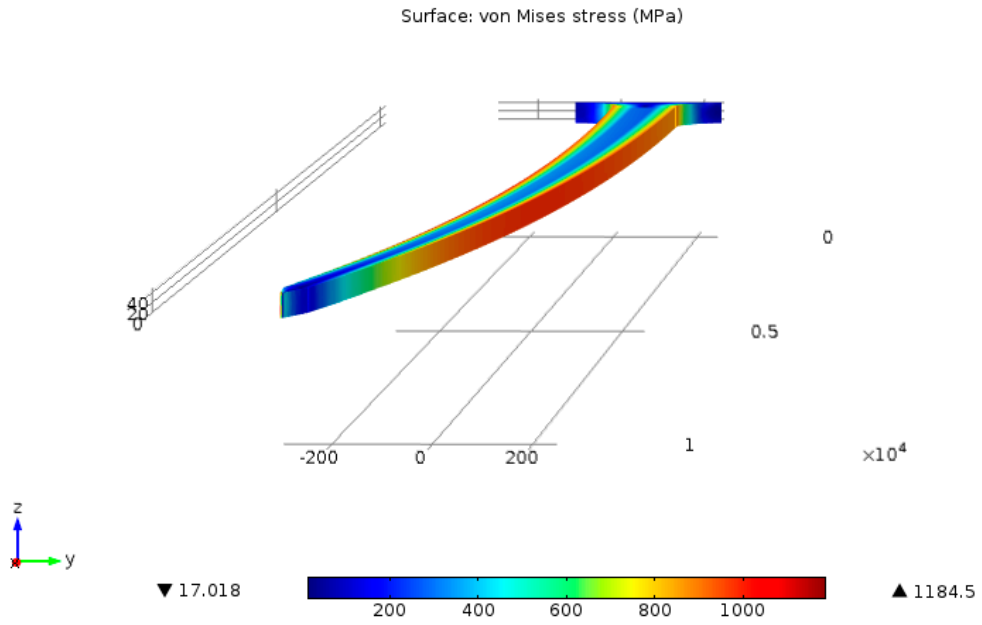

131

132 **Figure 3.** Behavior of non-porous probe under compression force along x and y of 756 MPa causing
133 the induction of the failure stress 1GPa.

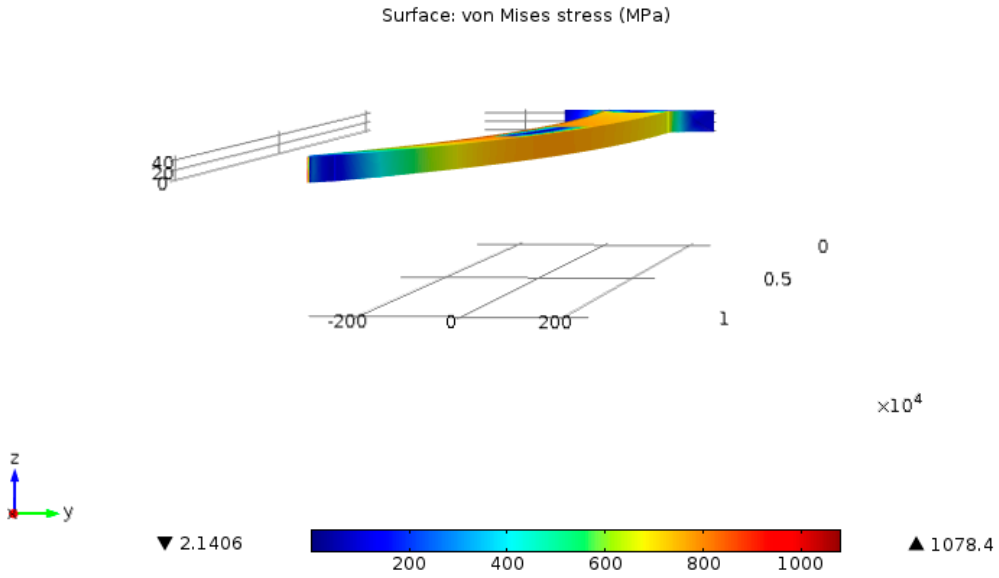

134

135 **Figure 4.** Behavior of porous probe under compression force along x and y of 753.7 MPa causing the
136 induction of the failure stress 1GPa.

Preprints (www.preprints.org) | NOT PEER-REVIEWED | Posted: 9 January 2018 doi:10.20944/preprints201801.0080.v1

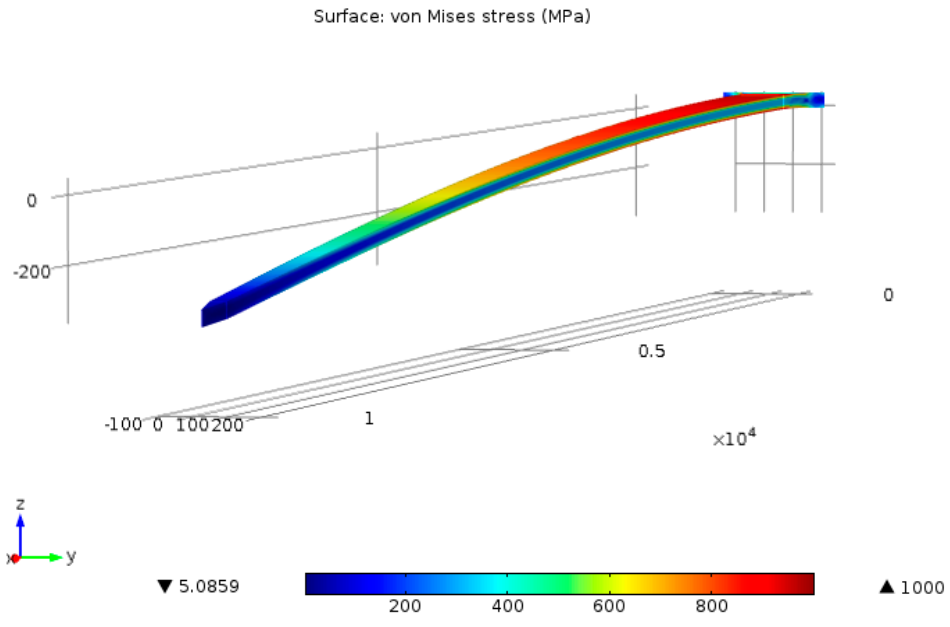

137

138 **Figure 5.** Behavior of non-porous probe under vertical force along negative z-axis of 36.5 MPa causing
139 the induction of the failure stress 1Gpa.

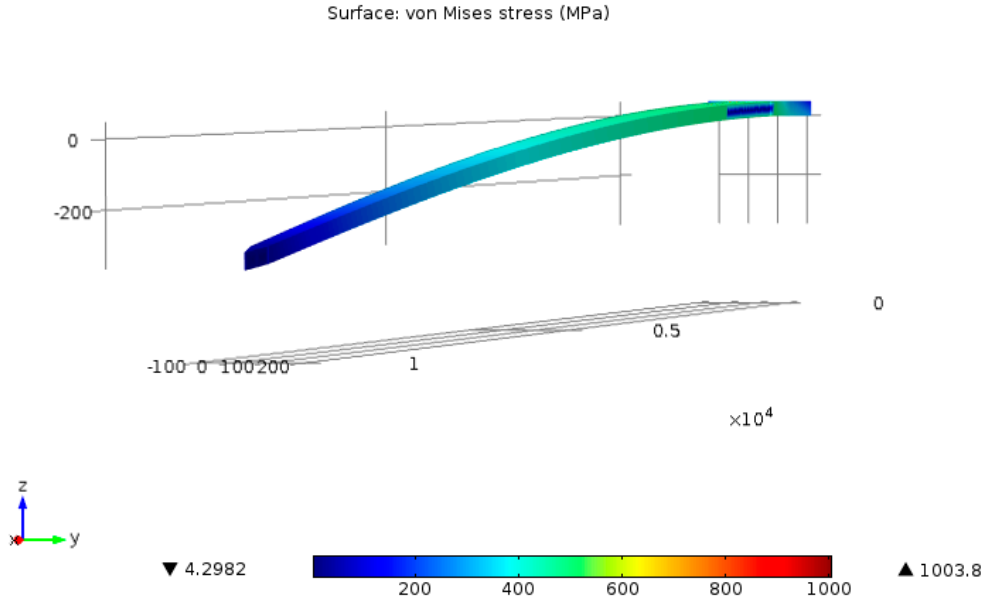

140

141 **Figure 6.** Behavior of porous probe under vertical force along negative z-axis of 23 MPa causing the
142 induction of the failure stress 1 Gpa.

143

Preprints (www.preprints.org) | NOT PEER-REVIEWED | Posted: 9 January 2018 doi:10.20944/preprints201801.0080.v1

Table 1. Comparison of stresses imposed on porous and non-porous probes in the three different cases (Area of application = 50 μm x 10 μm)

Case	Non-Porous (MPa)	Resultant Von-Mises (MPa)	Porous (Applied MPa)	Resultant Von-Mises (MPa)
Case 1: During implantation procedure	756	1184.5	753.7	1078.4
Case 2: Instantly after implantation procedure	1055	1049.9	1045	1046
Case 3: After implantation and during usage (with brain movement)	36.5	1047.9	23	1228

4. Microfabrication Process

The microfabrication process for the non-porous probe array has been described in detail in our previous publication [19]. In the current work, the microfabrication process follows similar steps at the beginning to form the probe array structure. During the end of the process, we perform additional processing to obtain porous probes. In brief, the microfabrication process begins with dicing a 50 μm thick 4" diameter double side polished silicon wafer (boron doped, resistivity of 20 ohm-cm and <100> oriented) into small square pieces by using a dicing saw. Metal layers of titanium (adhesion layer, 500 nm thick) and gold (conducting layer, 750 nm thick) are then deposited by sputtering process on the silicon wafer as depicted in Figure 7 (a). The gold and titanium layers are photolithographically patterned and wet etched, with solutions of 1:2:10 I_2:KI:H_2O and 20:1:1 H_2O:HF:H_2O_2, respectively, to define the recording pads, interconnects between the recording sites, and bonding pads as illustrated in Figure 7(b). The silicon substrate was then patterned using photolithography and etched using isotropic xenon difluoride (XeF_2) dry etching system to form the probe structures as illustrated in Figure 7(c). The photoresist mask used in the previous step is removed and the silicon probe array is exposed etched using isotropic XeF_2 dry etching system to form porous surfaces on the probe array. The formation of porous silicon using XeF_2 dry etching system is described in our previous publications [33-35].

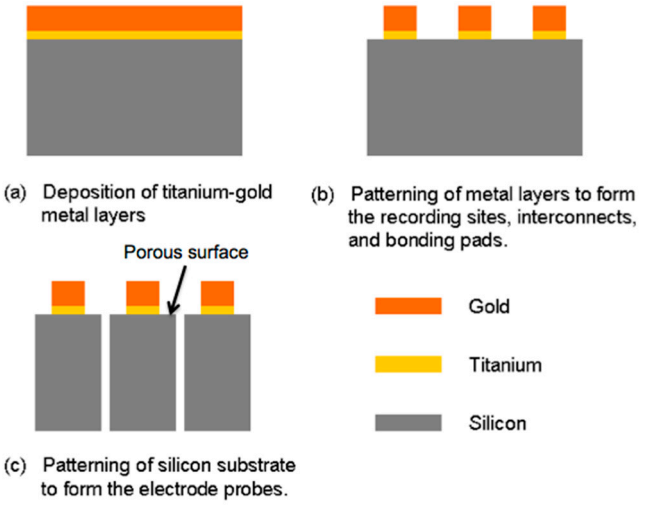

Figure 7: Schematic illustration of the steps involved in the fabrication process of the neural probe array. The figure is not to scale.

Preprints (www.preprints.org) | NOT PEER-REVIEWED | Posted: 9 January 2018 doi:10.20944/preprints201801.0080.v1

A 2µm thick layer of parylene-C, a biocompatible material widely used for coating a wide variety of implantable biomedical devices such as pacemakers and silicon [36] and metal-wire neural probes [3], is conformably deposited, at room temperature using a chemical vapor deposition (CVD) system, on the top side of the probe. It is mainly used to insulate the interconnects between the recording sites and bonding pads. Openings to expose the recording sites (used to measure the neural electrical activities) and the bonding pads (for wire-bonding to an external printed circuit board (PCB) for read-out) were defined with photolithography. The exposed parylene-C is etched with oxygen plasma ashing system (PVA TePla Inc., Model: 200).

Figure 8(a) is close-up view of the probe probes clearly showing the chisel-shaped tip, the titanium-gold recording site, and interconnects. Figures 8(b) is a magnified top view of the probe showing the porous silicon area around the recording sites. Figure 8(c) show magnified views of one recording site before and after etching the parylene-C to expose 10 µm x 10 µm gold recording site. Deposition and etching of parylene-C was performed before nanotexturing the probes with XeF_2. The bonding pads used to connect the recording sites to external circuitry are shown in Figure 8(d).

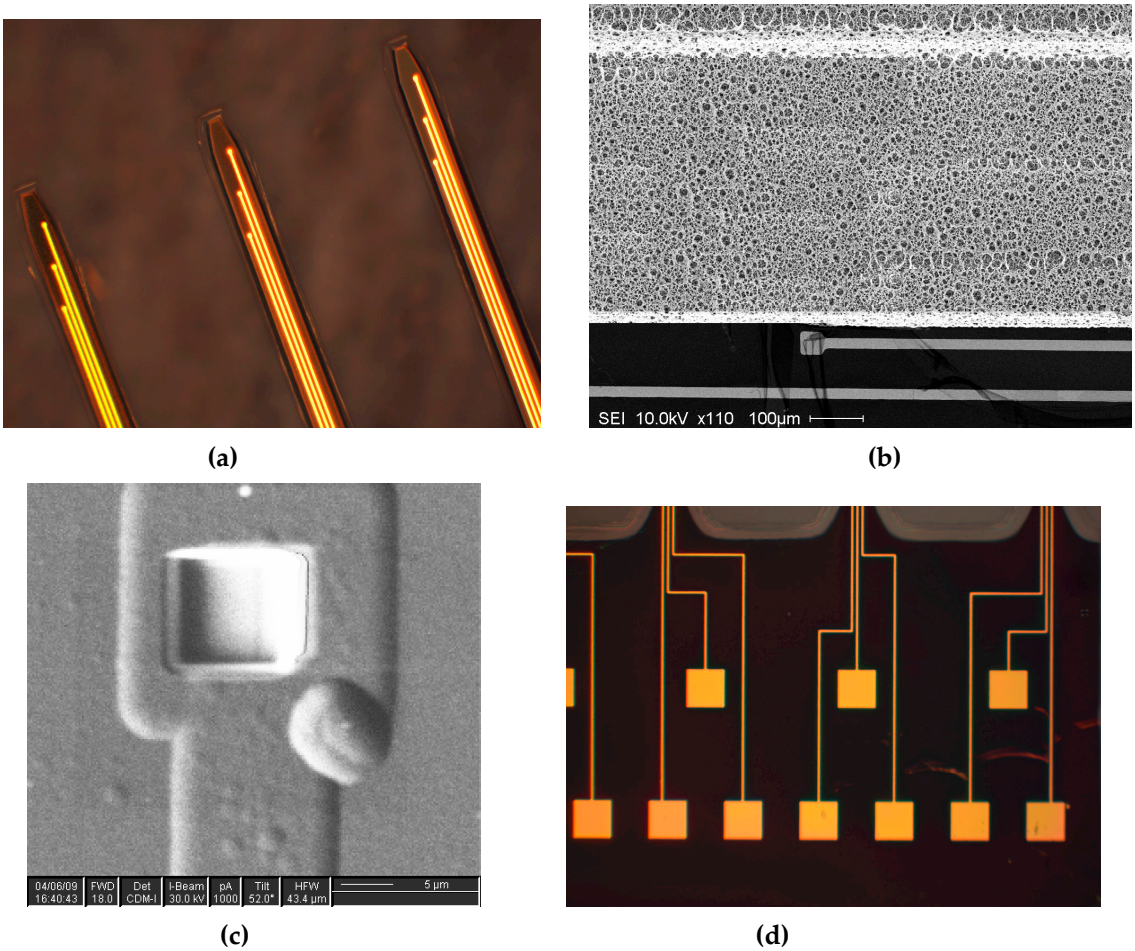

(a) **(b)** **(c)** **(d)**

Figure 8. Images of the fabricated porous neural probe array. **(a)** Close-up image of the probe probes; **(b)** Images of the neural probe with recording probe and porous surface; **(c)** A recording site after etching parylene-C; **(d)** Bonding pads.

The recording probe impedance is critical in the design of neural probes and is dominated by the size of the recording probe site. The values of the impedance of the recording sites are obtained by recording the electric current while submerging the neural probes in saline solution and injecting current through them. Figure 9 shows the measured impedance for the twelve recording sites

Preprints (www.preprints.org) | NOT PEER-REVIEWED | Posted: 9 January 2018 doi:10.20944/preprints201801.0080.v1

forming the current neural probe at 1 kHz and was found to be approximately 500 kΩ, a suitable impedance to record both single neuron activity and local field potentials (LFPs) [3].

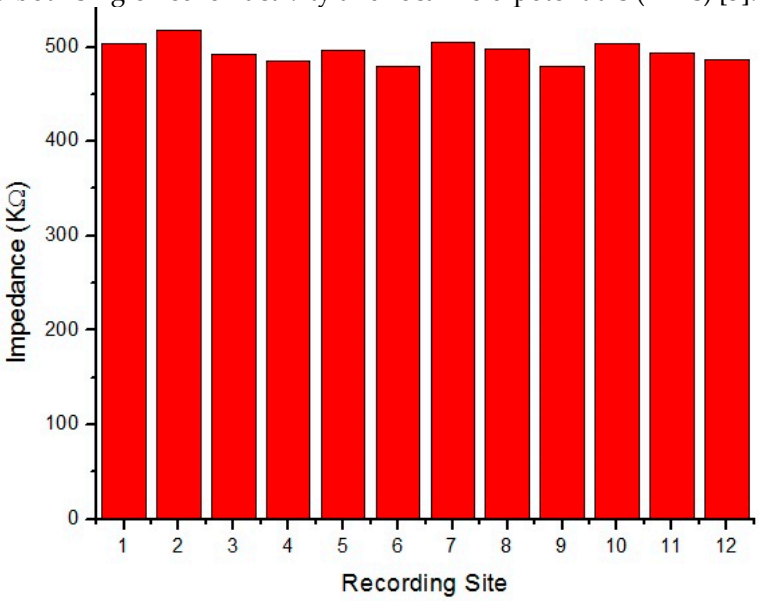

Figure 9. Impedance of the recording sites at 1 KHz.

5. Testing and Results

The developed neural probe was tested in the barrel cortex of a rat. All procedures were approved by the McGill University Animal Care Committee on May 18, 2010 and were also in compliance with the guidelines of the Canadian Council on Animal Care. The protocol number is 5314. A Sprague–Dawley rat was handled for several days before the surgery in order to accustom it to handling by the investigators. We tested the probe array in the barrel cortex of a rat using a procedure described previously by [3]. Our target was subcortical nuclei. The probe was centered at 3mm lateral and 2 mm anterior of the bregma and lowered 100-200 micron steps to a depth of 5mm. The dura of the rat was not dissected prior to silicon probe insertion. A thin silver wire was placed under the skin and attached to a screw in the skull for use as an additional ground. The rat was given pain, anti-inflammatory and antibiotic medication as directed by our protocol and the McGill veterinarian. The rat was allowed to recover for at least 1 week before recordings were performed.

Spiking activity was recorded using a multi-channel acquisition processor (MAP, Plexon Inc., Dallas, TX, USA) where single units were isolated online using time–voltage windows and their timing and spike waveforms stored on computer. Figure 10(a) shows recordings from six recording sites of the developed neural probe array. Action potential waveforms from multiple neurons are visible in the signal. In particular, several action potential waveforms, or "spikes," from two neurons, were detected in the neural signal as recorded by the first and the fifth recording sites. Local field potentials (LFPs) were recorded simultaneously from the same recording sites as shown in Figure 10(b). Multiple implantations are planned to gauge longevity of recordings.

Preprints (www.preprints.org) | NOT PEER-REVIEWED | Posted: 9 January 2018 doi:10.20944/preprints201801.0080.v1

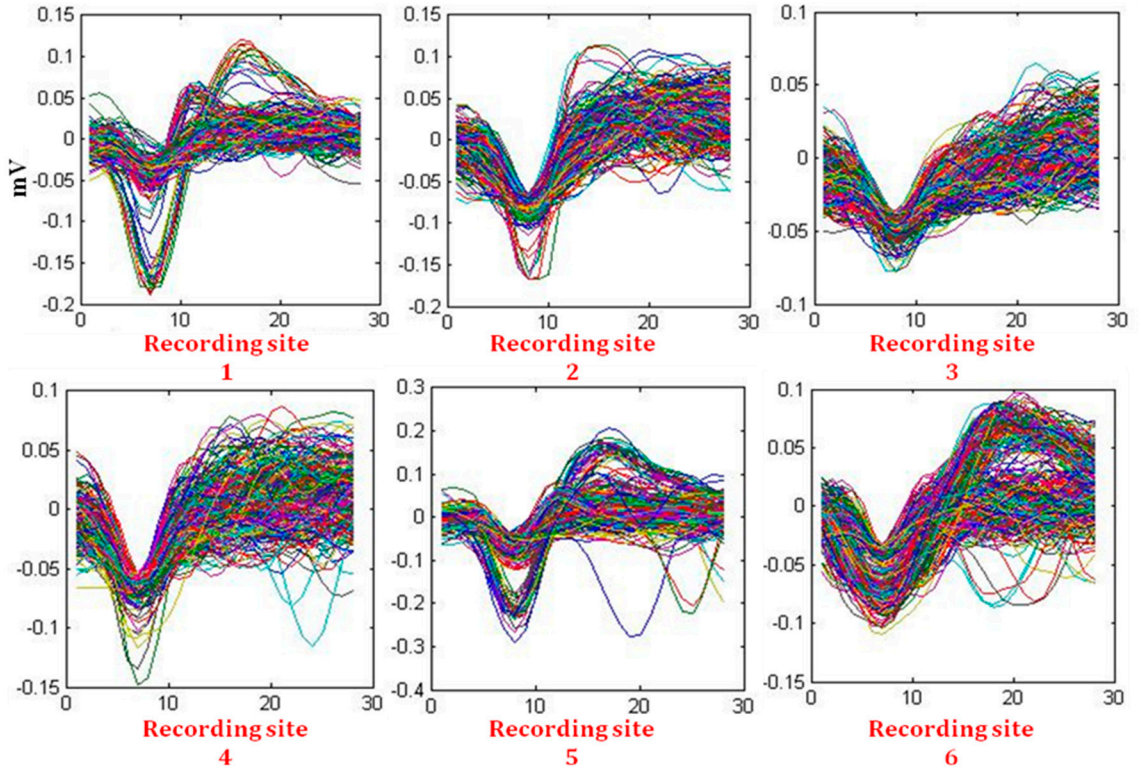

(a)

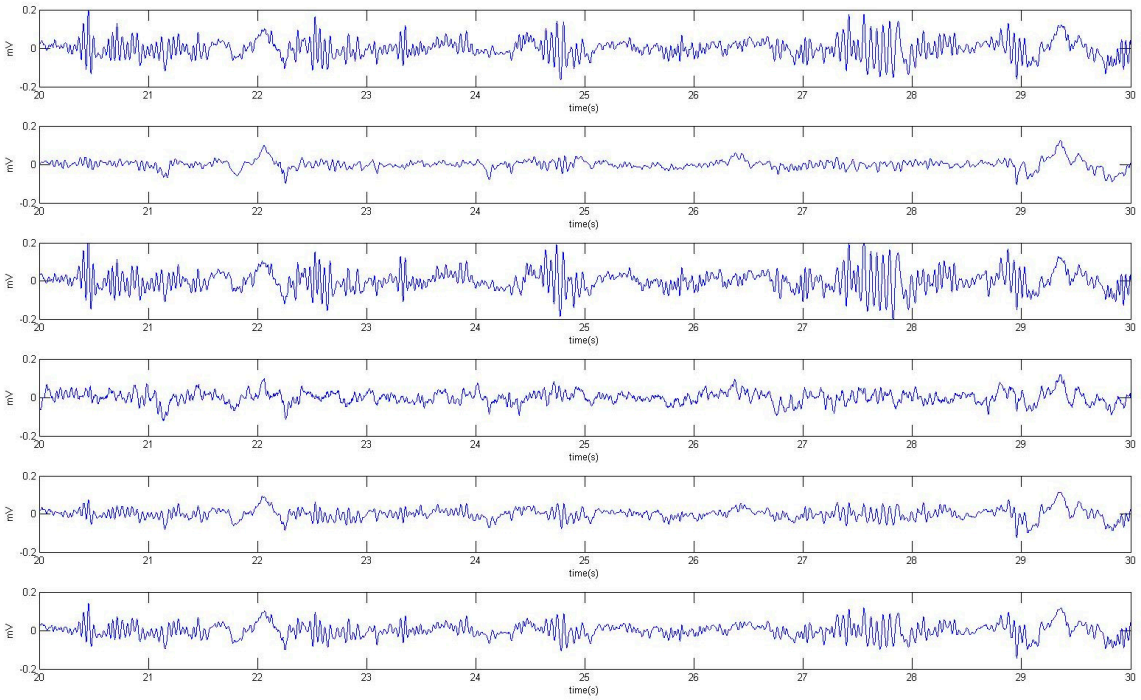

(b)

Figure 10. Neural recordings from six recording sites from the developed neural probe array

6. Conclusions

The goal of the work reported here is to prove the functionality of the developed neural probe in accurately recording neural activity. We described a novel methodology to fabricate elongated multi-

site neural microprobes with porous silicon surface using XeF_2 dry etching. The neural probes with porous surface can help to host neural growth factors to reduce immune response from brain improving biocompatibility and the adherence to the surrounding neural tissue. The probes were inserted through the pia and cortex of live rats to test their penetration ability. Results show a full insertion of the probes was successful without any bending, buckling, or breakage. Spiking activity and local field potentials (LFPs) were recorded simultaneously from the probes. Long-term implantation studies are required as subsequent work to investigate the effect of the porous silicon surface on the performance and function of the probe.

Acknowledgments: We would like to thank the financial support given by Natural Sciences and Engineering Research Council (NSERC) of Canada, Canadian Institutes for Health Research (CIHR), and the Canada Research Chair program. We would like to acknowledge the assistance of the McGill's Nanotools and Microfabrication Laboratory in preparing the described neural microprobe samples.

Author Contributions: Mohamad Hajj-Hassan and Vamsy Chodavarapu manufactured and tested electrical impedance of the neural probe. Rayan Fayad and Soumaya Berro conducted the numerical simulations. Sam Musallam tested the neural probes *in-vivo*.

Conflicts of Interest: "The authors declare no conflict of interest."

"The founding sponsors had no role in the design of the study; in the collection, analyses, or interpretation of data; in the writing of the manuscript, and in the decision to publish the results".

References

1. Andersen, R.A., E.J. Hwang, and G.H. Mulliken, *Cognitive Neural Prosthetics.* Annual Review of Psychology, 2010. **61**: p. 169-190.
2. Hatsopoulos, N.G. and J.P. Donoghue, *The science of neural interface systems.* Annu Rev Neurosci, 2009. **32**: p. 249-66.
3. Musallam, S., et al., *A floating metal microelectrode array for chronic implantation.* J Neurosci Methods, 2007. **160**(1): p. 122-7.
4. Williams, J.C., R.L. Rennaker, and D.R. Kipke, *Stability of chronic multichannel neural recordings: Implications for a long-term neural interface.* Neurocomputing, 1999. **26-7**: p. 1069-1076.
5. Kralik, J.D., et al., *Techniques for long-term multisite neuronal ensemble recordings in behaving animals.* Methods, 2001. **25**(2): p. 121-150.
6. Drake, K.L., et al., *Performance of Planar Multisite Microprobes in Recording Extracellular Single-Unit Intracortical Activity.* Ieee Transactions on Biomedical Engineering, 1988. **35**(9): p. 719-732.
7. Hetke, J.F., D.J. Anderson, and K.D. Wise, *Design ranges for silicon multichannel neural probes.* Proceedings of the 18th Annual International Conference of the Ieee Engineering in Medicine and Biology Society, Vol 18, Pts 1-5, 1997. **18**: p. 266-267.
8. Campbell, P.K., et al., *A silicon-based, three-dimensional neural interface: manufacturing processes for an intracortical electrode array.* IEEE Trans Biomed Eng, 1991. **38**(8): p. 758-68.
9. Kipke, D.R., et al., *Silicon-substrate intracortical microelectrode arrays for long-term recording of neuronal spike activity in cerebral cortex.* IEEE Trans Neural Syst Rehabil Eng, 2003. **11**(2): p. 151-5.
10. Hajj-Hassan, M., V. Chodavarapu, and S. Musallam, *Reinforced silicon neural microelectrode array fabricated using a commercial MEMS process.* Journal of Micro-Nanolithography Mems and Moems, 2009. **8**(3): p. 033011.
11. Z. Fekete, E. Pálfi, G. Márton, M. Handbauer, Zs. Bérces, I. Ulbert, A. Pongrácz, L. Négyessy, *In Vivo Iontophoretic BDA Injection through a Buried Microfluidic Channel of a Neural Multielectrode*, Procedia Engineering, 2015. **120**, Pages 464-467.

12. F. Michon, et al., *Integration of silicon-based neural probes and micro-drive arrays for chronic recording of large populations of neurons in behaving animals*, 2016. **13**(4).
13. He, W., et al., *A novel anti-inflammatory surface for neural electrodes.* Advanced Materials, 2007. **19**(21): p. 3529-3533.
14. Lee, H., et al., *Biomechanical analysis of silicon microelectrode-induced strain in the brain.* Journal of Neural Engineering, 2005. **2**(4): p. 81-89.
15. Subbaroyan, J., D.C. Martin, and D.R. Kipke, *A finite-element model of the mechanical effects of implantable microelectrodes in the cerebral cortex.* Journal of Neural Engineering, 2005. **2**(4): p. 103-113.
16. Brien, D.P.O., T.R. Nichols, and M.G. Allen. *Flexible microelectrode arrays with integrated insertion devices*. in *Micro Electro Mechanical Systems, 2001. MEMS 2001. The 14th IEEE International Conference on*. 2001.
17. Rousche, P.J. and R.A. Normann, *A method for pneumatically inserting an array of penetrating electrodes into cortical tissue.* Ann Biomed Eng, 1992. **20**(4): p. 413-22.
18. HajjHassan, M., V. Chodavarapu, and S. Musallam, *NeuroMEMS: Neural Probe Microtechnologies.* Sensors, 2008. **8**(10): p. 6704-6726.
19. Hajj-Hassan, M., V.P. Chodavarapu, and S. Musallam, *Microfabrication of ultra-long reinforced silicon neural electrodes.* Micro & Nano Letters, 2009. **4**(1): p. 53-58.
20. Bridges, A.W., et al., *Chronic inflammatory responses to microgel-based implant coatings.* J Biomed Mater Res A, 2010. **94**(1): p. 252-8.
21. Szarowski, D.H., et al., *Brain responses to micro-machined silicon devices.* Brain Res, 2003. **983**(1-2): p. 23-35.
22. Turner, J.N., et al., *Cerebral astrocyte response to micromachined silicon implants.* Exp Neurol, 1999. **156**(1): p. 33-49.
23. Ludwig, K.A., et al., *Chronic neural recordings using silicon microelectrode arrays electrochemically deposited with a poly(3,4-ethylenedioxythiophene) (PEDOT) film.* Journal of Neural Engineering, 2006. **3**(1): p. 59-70.
24. McConnell, G.C., et al., *Implanted neural electrodes cause chronic, local inflammation that is correlated with local neurodegeneration.* J Neural Eng, 2009. **6**(5): p. 056003.
25. Kozai, T.D., et al., *Ultrasmall implantable composite microelectrodes with bioactive surfaces for chronic neural interfaces.* Nat Mater, 2012. **11**(12): p. 1065-73.
26. Kim, D.H., M. Abidian, and D.C. Martin, *Conducting polymers grown in hydrogel scaffolds coated on neural prosthetic devices.* J Biomed Mater Res A, 2004. **71**(4): p. 577-85.
27. Kim, D.H., et al., *Soft, Fuzzy, and Bioactive Conducting Polymers for Improving the Chronic Performance of Neural Prosthetic Devices*, in *Indwelling Neural Implants: Strategies for Contending with the In Vivo Environment*, W.M. Reichert, Editor. 2008: Boca Raton (FL).
28. Wadhwa, R., C.F. Lagenaur, and X.T. Cui, *Electrochemically controlled release of dexamethasone from conducting polymer polypyrrole coated electrode.* J Control Release, 2006. **110**(3): p. 531-41.
29. Howell, B. and W.M. Grill, *4 - Design of electrodes for stimulation and recording A2 - Kilgore, Kevin*, in *Implantable Neuroprostheses for Restoring Function*. 2015, Woodhead Publishing. p. 59-93.
30. Bartels, J., et al., *Neurotrophic electrode: Method of assembly and implantation into human motor speech cortex.* Journal of Neuroscience Methods, 2008. **174**(2): p. 168-176.
31. Thompson, C.H., et al., *Regenerative Electrode Interfaces for Neural Prostheses.* Tissue Engineering Part B-Reviews, 2016. **22**(2): p. 125-135.
32. Hajj-Hassan, M., et al., *Response of murine bone marrow-derived mesenchymal stromal cells to dry-etched porous silicon scaffolds.* Journal of Biomedical Materials Research Part A, 2011. **99a**(2): p. 269-274.

316 33. Hajj-Hassan, M., M. Cheung, and V. Chodavarapu, *Dry etch fabrication of porous silicon using xenon*
317 *difluoride*. Micro & Nano Letters, 2010. **5**(2): p. 63-69.
318 34. Hajj-Hassan, M., M.C. Cheung, and V.P. Chodavarapu, *Ultra-thin porous silicon membranes fabricated*
319 *using dry etching*. Micro & Nano Letters, 2011. **6**(4): p. 226-228.
320 35. Cheung, M.C.K., et al., *Controlling optical properties and surface morphology of dry etched porous silicon (vol*
321 *5, 053503, 2011)*. Journal of Nanophotonics, 2011. **5**.
322 36. Hsu, J.M., et al., *Encapsulation of an Integrated Neural Interface Device With Parylene C*. Ieee Transactions
323 on Biomedical Engineering, 2009. **56**(1): p. 23-29.
324